

## Article

# Nano- and Submicron-Sized TiB<sub>2</sub> Particles in Al–TiB<sub>2</sub> Composite Produced in Semi-Industrial Self-Propagating High-Temperature Synthesis Conditions

Aleksey Matveev<sup>1,2,\*</sup>, Vladimir Promakhov<sup>1</sup>, Nikita Schulz<sup>1</sup>, Vladislav Bakhmat<sup>1</sup> and Timur Turanov<sup>1</sup>

- <sup>1</sup> Scientific and Educational Center “Additive Technologies”, National Research Tomsk State University, Lenin Avenue, 36, 634050 Tomsk, Russia; vvpromakhov@mail.ru (V.P.); schulznikita97@gmail.com (N.S.); bakhmatvr@gmail.com (V.B.); timur.kb2@icloud.com (T.T.)
- <sup>2</sup> Tomsk Scientific Center of the Siberian Branch of the Russian Academy of Sciences, 10/4, Akademicheskii Ave., 634055 Tomsk, Russia
- \* Correspondence: alekey.9595@mail.ru; Tel.: +7-9095484574

**Abstract:** This paper investigates the structure and phase composition of Al–TiB<sub>2</sub> metal matrix composites prepared from the Al–Ti–B system powder using self-propagating high-temperature synthesis (SHS) in semi-industrial conditions (the amount of the initial powder mixture was 1000 g). The samples produced in semi-industrial conditions do not differ from the laboratory samples, and consist of the aluminum matrix and TiB<sub>2</sub> ceramic particles. The temperature rise leads to the growth in the average size of TiB<sub>2</sub> particles from 0.4 to 0.6 μm as compared to the laboratory samples. SHS-produced composites are milled to the average particle size of 42.3 μm. The powder particles are fragmented, their structure is inherited from the SHS-produced Al–TiB<sub>2</sub> metal matrix composite. The obtained powder can be used as the main raw material and additive in selective laser sintering, vacuum sintering, and hot pressing products. It is worth noting that these products can find their own application in the automotive industry: brake pads, drums, rail discs, etc.



**Citation:** Matveev, A.; Promakhov, V.; Schulz, N.; Bakhmat, V.; Turanov, T. Nano- and Submicron-Sized TiB<sub>2</sub> Particles in Al–TiB<sub>2</sub> Composite Produced in Semi-Industrial Self-Propagating High-Temperature Synthesis Conditions. *Metals* **2024**, *14*, 511. <https://doi.org/10.3390/met14050511>

Academic Editors: Tomasz Tański, Andrzej N. Wiczorek and Marcin Staszuk

Received: 12 March 2024  
Revised: 19 April 2024  
Accepted: 23 April 2024  
Published: 28 April 2024



**Copyright:** © 2024 by the authors. Licensee MDPI, Basel, Switzerland. This article is an open access article distributed under the terms and conditions of the Creative Commons Attribution (CC BY) license (<https://creativecommons.org/licenses/by/4.0/>).

**Keywords:** Al–TiB<sub>2</sub> metal matrix composites; self-propagating high-temperature synthesis; semi-industrial conditions; synthesis process; structure and phase composition; nanoparticles

## 1. Introduction

Transportation of people and cargo by air, land, and water transport must meet modern economic and environmental requirements [1]. One of these requirements is a lower weight of structural elements of transport, which improves the transportation performance, fuel saving, and reduces harmful gas emissions [2,3]. For example, an aircraft weight reduction by 20% decreases the CO<sub>2</sub> emission by 12–16%, which undoubtedly has a positive effect on the environment and humans. The reduction of the weight indicators of the transport structure can be gained not only by design improvements, but also by the development and implementation of novel materials. The structure and phase composition of novel materials can significantly improve their physical and mechanical properties (relative to present materials) and provide stable operation at higher temperatures. The creation of metal matrix composites, comprising a metal/intermetallic matrix and ceramic particles, is currently one of the key trends in the development of novel materials [4–6]. Dispersion hardening of metal matrix materials by ceramic particles enhances their physical and mechanical properties, namely hardness, wear resistance, and strength both at room and higher temperatures [7,8]. On the other hand, nano- and submicron-sized ceramic particles are also nucleation centers of crystalline particles in metal alloys that reduce their grain size and improve their physical and mechanical properties [9–12]. It should be noted that ordinary alloys cannot reach the physical and mechanical properties of the metal matrix composites, owing to their more free growth of crystalline particles.

It is thanks to the unique combination of physical and mechanical properties that metal matrix composites have found applications in the automotive industry: brake pads, drums, rail discs, etc. At the same time, intensive growth in the production of passenger cars is expected (for example, in the Asia–Pacific region, automobile production increased by 11%). Based on these data, it is assumed that the production of parts for passenger cars will be one of the main drivers of growth in the market for composite metal matrix materials. According to work [13], in 2020, the global market for metal matrix composites and materials based on them is estimated at USD 360 billion. It is projected to grow at a CAGR of 6.4% from 2020 to 2027. There are currently many ways to obtain metal matrix composites; for example, the addition of ceramic particles in the melt, hot pressing, and spark plasma sintering [14–16]. A special focus is the self-propagating high-temperature synthesis (SHS) technique based on exothermic reactions between mixture components. SHS is characterized by highly intensive interactions between initial components, which are accompanied by large amounts of generated heat [17]. This amount of heat avoids the necessity for using external energy sources during synthesis. Moreover, the SHS technique ensures control over the structure and phase composition of synthesis products by changing the initial mixture composition and reaction conditions. For metal matrix composites, the SHS process provides for in situ structure formation, i.e., during the reaction between the initial mixture components. In this case, the heat of reaction between ceramic particles is spent to the metal component melting. At high (>40 wt.%) content, ceramic particles are separated by the obtained alloy, which forms the matrix material. This largely eliminates the particle agglomeration and allows producing composite materials with a homogeneous structure [18].

Using SHS, the research team headed by prof. Promakhov has obtained (Ni–Ti)–TiB<sub>2</sub> composite from the powder system 63.5 wt.% NiB + 36.5 wt.% Ti [19]. The composite structure consisted of the Ni–Ti intermetallic matrix with distributed particles of titanium diboride (TiB<sub>2</sub>). It was found that the addition of 5 wt.% SHS-particles NiTi–TiB<sub>2</sub> to the Inconel 625 powder enhanced the hardness and ultimate tensile strength of SLS materials, respectively, by 40 and 20% as compared to relatively pure Inconel 625 powder [20]. These results demonstrated the highly efficient use of SHS-produced composites as additives in selective laser sintering.

According to the literature review, most of the publications in the field of composites do not go beyond the laboratory experiments. There are experiments with 20 to 50 g samples, in which synthesis conditions considerably differ from the production process conditions and do not consider process and ecological parameters. As mentioned above, the main research tasks include the development of composite materials and their industrial implementations. The SHS technique is, therefore, the focus of attention; semi-industrial conditions may significantly affect the structure and phase composition and, consequently, the physical and mechanical properties of the final product.

In work [18], SHS was used to obtain the Al–TiB<sub>2</sub> metal matrix composite from the Al–Ti–B system powder in laboratory conditions. The composite structure consisted of the aluminum matrix with uniformly distributed TiB<sub>2</sub> particles submicron and nanometer size.

Note that it is nano- and submicron-sized ceramic particles that provide the improvement of physical and mechanical properties for unavailable conventional aluminum and many other alloys. Thus, the obvious question that arises is whether it is possible to gain such results when increasing the weight of the initial powder mix up to 1000 g (1 kg) and approaching semi-industrial SHS conditions.

The aim of this work is to investigate the structure and phase composition of the Al–TiB<sub>2</sub> metal matrix composite produced by SHS from the Al–Ti–B system powder in semi-industrial conditions.

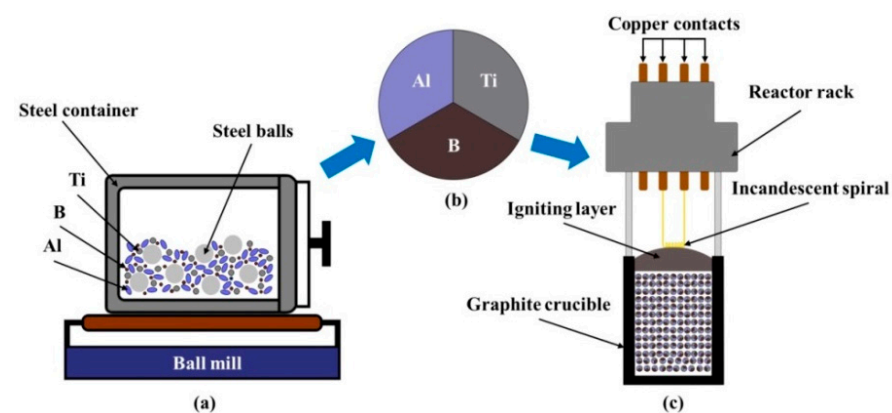
## 2. Materials and Methods

Aluminum (Al), titanium (Ti), and boron (B) powders were used to prepare 1000 g (1 kg) of the Al–Ti–B system powder. Table 1 shows manufacturers, average particle size, and purity of these powders.

**Table 1.** Manufacturers, average particle size, and purity of powders.

Powders	Average Particle Size, $\mu\text{m}$	Purity, wt.%
Al (OOO Sual-PM)	100	$\geq 98.4$
Ti (OAO Polema)	140	$\geq 99$
B (OAO Aviabor)	0.6	$\geq 99.2$

The initial powder components were mixed with the amount of 60 wt.% Al, 27.6 wt.% Ti, and 12.4 wt.% B. The obtained mixture was mechanically blended in the ball mill, as illustrated in Figure 1a. To understand how the duration of mechanical grinding affects the particle structure of the initial powder mixture weighing 1000 g, two mechanical grindings were carried out: 15 min (as presented in [18] for a sample weighing 20 g), and 45 min. The steel drum was vacuumed and filled with argon to prevent the contents oxidation. Based on the data obtained in the work [21], it was supposed that after mechanical blending, the initial powder mix consisted mostly of composite particles with Al, Ti, and B inclusions (Figure 1b). Next, this powder mix was poured into a graphite crucible without preliminary compaction. A flammable layer comprising 80 wt.% Ti and 20 wt.% B was poured onto the powder mix. The flammable layer provided uniform heating of the upper layer of the main mix and initiated the reaction between the components. The graphite crucible was placed in the reactor (Figure 1c).



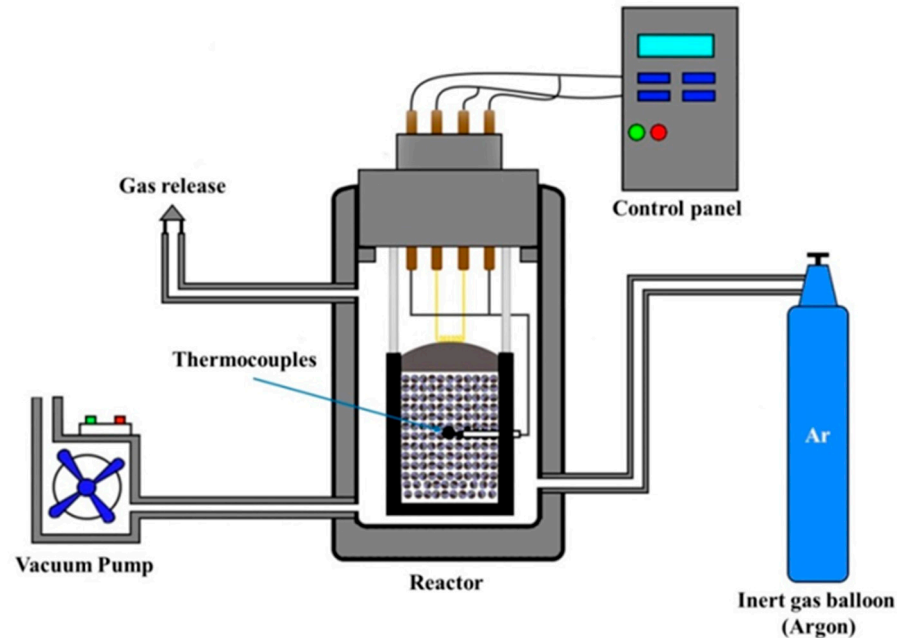
**Figure 1.** Flowchart of Al–Ti–B based sample preparation: (a) ball mill, (b) Al, Ti, and B particles, (c) reactor.

Figure 2 presents semi-industrial conditions in the SHS process. The reactor was evacuated by a pump and filled with argon to a pressure of 5 MPa. The synthesis reaction was initiated by the localized heating of the flammable layer using a molybdenum hot filament. BP20/5 thermocouples were introduced in the initial powder mix to measure the synthesis temperature [22].

After synthesis, 1 kg of the obtained product was ground in a ball mill. A porcelain container and  $\text{Al}_2\text{O}_3$  balls of diameters 10 and 20 mm, respectively, were used for the grinding. The ground synthesis product was sieved through 200 mesh sieve.

The X-ray diffraction (XRD) analysis of the phase composition was conducted on a Shimadzu XRD-6000 Diffractometer (Shimadzu Corporation, Kyoto, Japan) using  $\text{CuK}\alpha$  radiation. The phase composition was identified by using the Powder Diffraction File (PDF-4). Rietveld refinement was used for the phase quantification and lattice parameters [23,24]. Energy dispersive X-ray spectroscopy on the scanning electron microscope (SEM/EDX)

with focused electron beam from Tescan (Tescan, s.r.o., Brno, Czech Republic) was used to study the sample microstructure. Its particle size was detected in SEM images using the secant method. The ANALYSETTE 22 MicroTec plus analyzer (Fritsch, Idar-Oberstein, Germany) was used to detect the particle size of the ground synthesis product.



**Figure 2.** Flowchart of semi-industrial SHS process.

### 3. Results

#### 3.1. Influence of the Powder Mix Weight and Synthesis Conditions on Its Temperature and Propagation

Figure 3 contains SEM images of the initial Al–Ti–B powder structure after mechanical blending for 15 and 45 min. After 15 min, the structure consists of deformed particles with Al, Ti, and B inclusions (see Figure 3a, regions 1, 3, 4, 6, 9). There are also rounded Al and Ti inclusions without boron (regions 2, 5, 7, 8). After 45 min, the structure includes planes and irregular particles (Figure 3b). According to the elemental analysis, they comprise Al and B inclusions (Figure 3b, regions 1–9). These results are consistent with those obtained in [18], where a similar particle structure is obtained after 15 min mechanical blending of 20 g Al–Ti–B powder. Thus, a larger weight of the initial powder mix requires longer mechanical blending.

In Figure 4, we present thermal curves for synthesis of 1000 g (1 kg) of the initial powder. The peak 1 on these curves describes the exothermic reaction between the initial powder components, which is accompanied by a large amount of generated heat. This peak corresponds to synthesis at 1850 °C. A comparison of results obtained here and in [18] shows that the SHS temperature grows by 200 °C with increasing weight of the Al–Ti–B system powder from 20 to 1000 g. This temperature rise is determined mostly by the larger diameter of the initial powder sample and, consequently, the reacting surface of its components. This results in a large amount of generated heat and temperature growth. The same was observed by Borovinskaya et al. [25], who detected the relation between the temperature and the sample dimension in several systems (for example, in Ti–B, Ti–2B, Ti–C, etc.). It should be noted that the initial powder mix was poured into the graphite crucible without a preliminary compaction (bulk density).

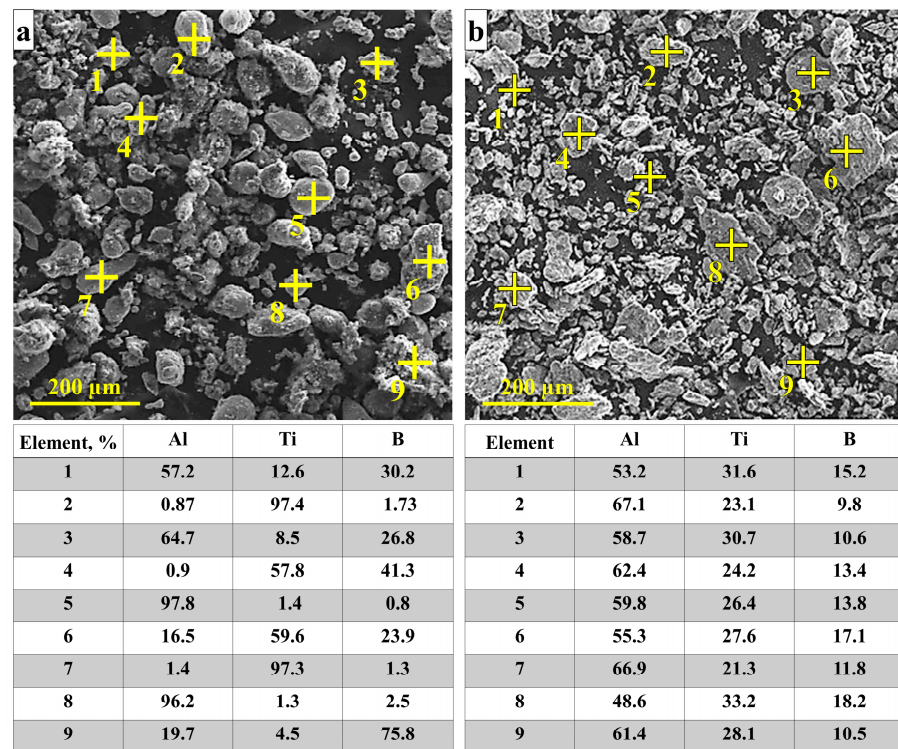


**Figure 3.** SEM images of 1000 g of initial Al–Ti–B system powder and elemental composition after mechanical blending: (a) 15 min, (b) 45 min.

At the same time, the density of powder samples obtained by cold uniaxial compaction in [18] from 20 g of the Al–Ti–B powder was higher than the bulk density. Yeh and Chen [26] reported that the SHS temperature grew with increasing density of the initial sample. However, in our experiment, the SHS temperature in the Al–Ti–B system powder with the bulk density and 1000 g weight was higher than that of the powder with 20 g weight. As mentioned above, the increase in the weight and volume of the initial powder mix led to the growth in the heat generation during the synthesis process due to the larger reacting surface. It was assumed that this heat compensated for the lower contact between the powder components associated with the reduced density of the initial powder mix that accompanied the higher temperature than in laboratory conditions. This allowed us to conduct stability and complete synthesis in conditions approaching semi-industrial ones, i.e., without preliminary compaction of the initial powder mix.

In Figure 4a, the temperature slightly lowers after peak 1 and then grows again (peak 2). This is conditioned by the intense heat absorption in the adjacent regions, where the remaining amount of heat results in the temperature growth. This phenomenon is detected in [27]: it is reported that endothermic processes are stipulated by the melting and dissolution of the initial mixture components. Afterwards, the temperature drops, and the synthesis product is cooled (region 3). The heat absorption by adjacent regions can cause wave front destabilization and spin wave propagation. It is noteworthy that the synthesis process conducted in the graphite crucible does not allow us to observe the wavefront propagation. At the same time, the surface of the synthesis product in Figure 4b,c has lines four separated by pores. Their formation can probably be attributed to localization reaction centers and their motion along a helical path. The temperature gradient appears on the boundaries of reaction centers and unreacted region, which results in the pore formation. These lines are typical for the spin wave propagation. Based on these data and the results obtained in [27], we find that the Al content of 60 wt.% of the initial Al–Ti–B system leads to an intense absorption of the large amount of heat necessary for its melting. This facilitates the wavefront destabilization and spin wave formation (Figure 4d, region 5). In work [18], the Al–Ti–B system powder, consisting of 60 wt.% Al and weighing 20 g, also demonstrates

the spin wave propagation during the synthesis process. In conclusion, the wavefront propagation in the Al–Ti–B system powder does not change with the weight of the initial powder mix increasing from 20 to 1000 g.

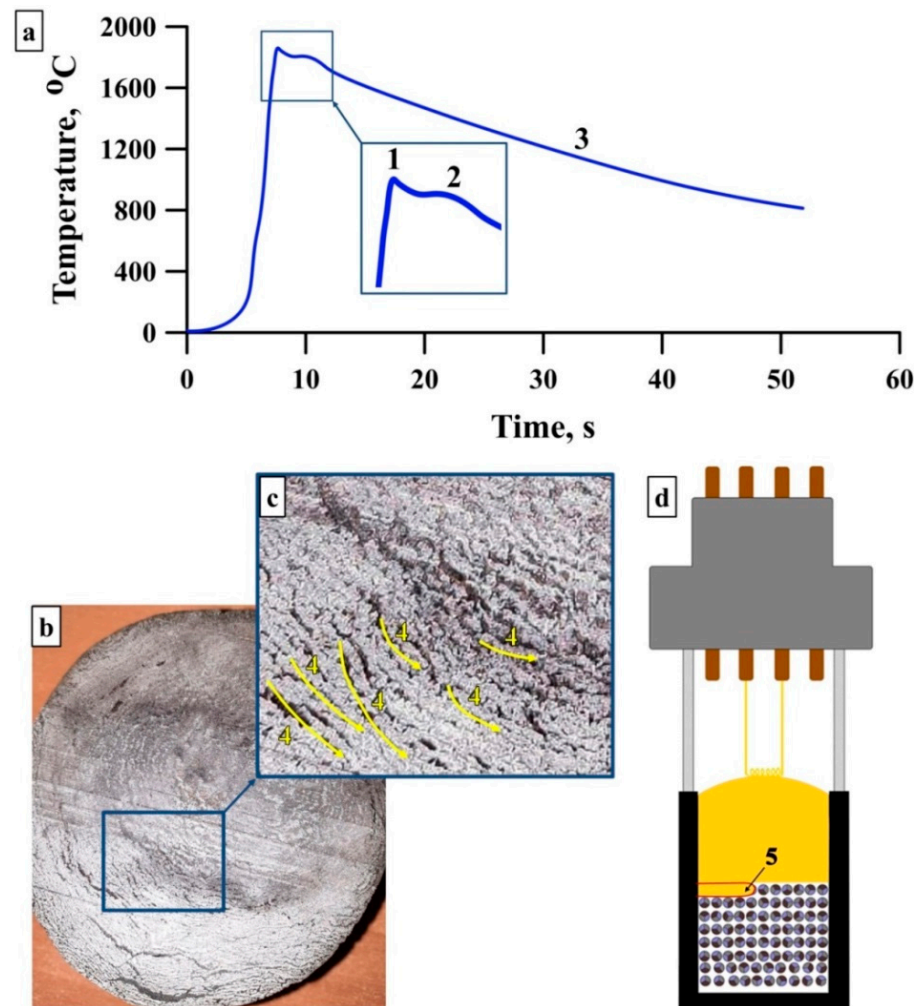


**Figure 4.** Thermal curves for 1000 g of Al–Ti–B system components (a), synthesis product surface (b,c), layerwise wave propagation in the initial powder mix (d).

### 3.2. Influence of the Powder Mix Weight and Synthesis Conditions on Structure and Phase Composition

The SEM images in Figure 5 demonstrate the structure of the SHS product preliminary treated in 5 vol.% HCl solution. The structure consists of irregular rounded particles (region 1) distributed in the matrix (region 2). The particle size ranges between 0.17 and 4  $\mu\text{m}$ , while the average size is 0.61  $\mu\text{m}$ . The particle size distribution is contributed largely by 0.5  $\mu\text{m}$  particles.

The XRD pattern and EDX mapping of the surface of SHS products obtained from the Al–Ti–B powder are presented in Figure 6. These products contain  $\text{TiB}_2$  and Al phases. Crystal lattice parameters of these phases do not qualitatively differ from each other and are comparable with those of reference Al and  $\text{TiB}_2$  phases [28,29]. There are also traces of the  $\text{Al}_3\text{Ti}$  intermetallic phase, while EDX mapping of the SHS product structure (Figure 6b–e) shows Ti and B elements nearby the detected particles. At the same time, the matrix consists of Al and also Ti elements in some areas.

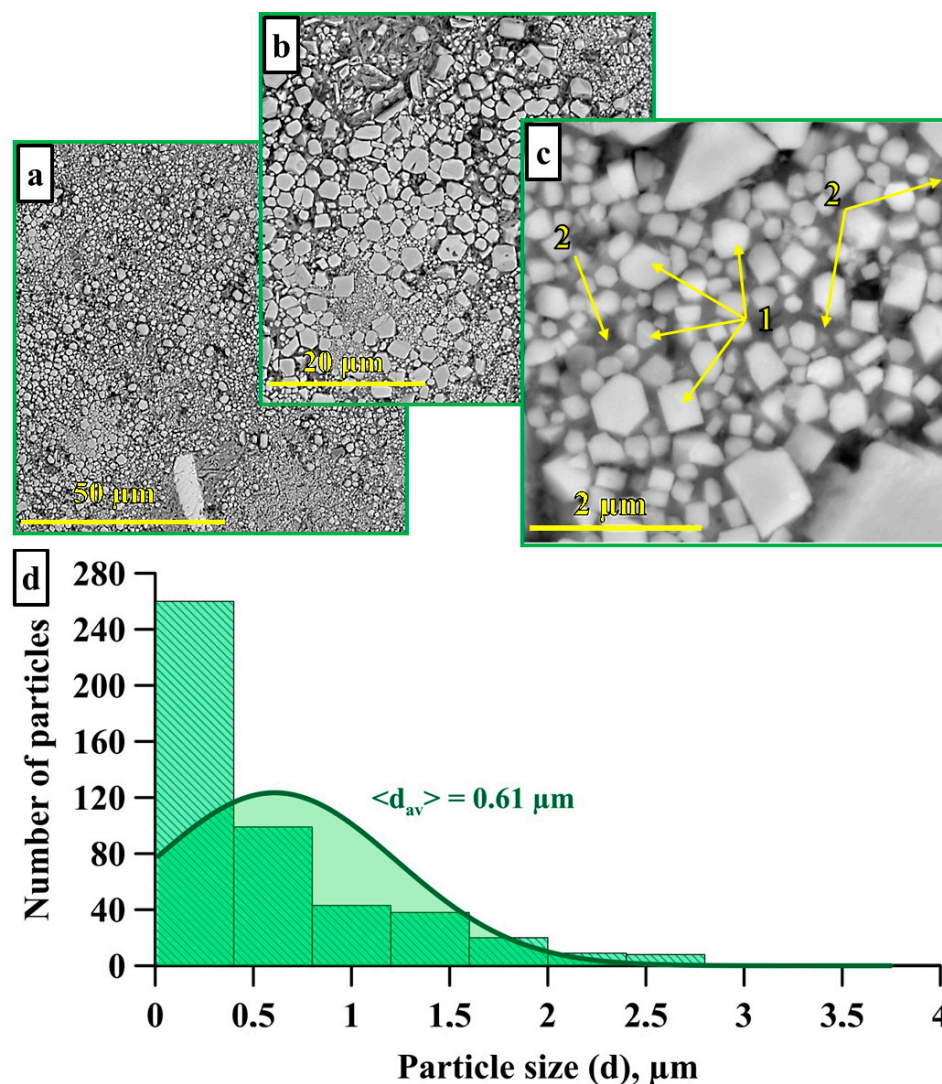


**Figure 5.** SEM images of the structure of SHS product with the weight of 1000 g (a–c) and particle size distribution in the matrix (d).

When comparing these data with XRD patterns, we found that SHS products, resulting from exothermic reactions from the Al–Ti–B system powder, consisted of  $\text{TiB}_2$  particles distributed in the matrix based on Al and  $\text{Al}_3\text{Ti}$  inclusions. When comparing these results with those achieved in [18] for 20 g of the initial powder mix, we observed a slight growth (from 0.4 to 0.6 μm) in the average size of  $\text{TiB}_2$  particles for 1000 g from the initial powder. That change was attributed to the temperature rise, which led to the growth in  $\text{TiB}_2$  crystalline particles and, thus, in the average particle size [30]. It is worthwhile to note that, in work [18], the synthesis of the Al–Ti–B system with 20 g weight did not result in the formation of Al–Ti intermetallic compounds. Based on the data presented herein, we suggested that the formation of intermetallic compounds was associated with a stoichiometry deviation during the mixture preparation with larger particle size. As a result of the results obtained, it was established that increasing the mass of the sample from 20 to 1000 g does not lead to a significant change in the phase composition and structure of the synthesis products. Therefore, it can be assumed that increasing the volume of the resulting mixture will not complicate the technological process, nor will it lead to economic costs.

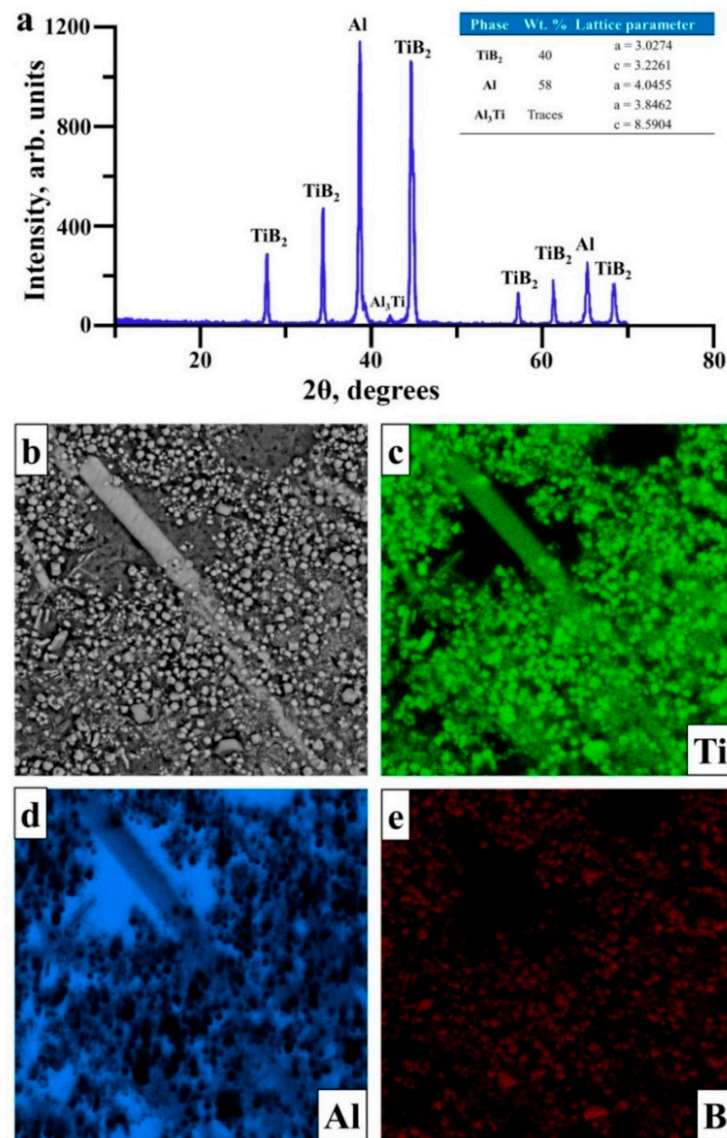


**Figure 6.** XRD pattern with phase composition (a) and EDX mapping (b–e) of SHS product obtained from 1000 g of the Al–Ti–B system powder.

As mentioned earlier, metal matrix composites can be used in selective laser sintering as the main powder material or additive. In this regard, after synthesis of 1000 g of the ceramic sample, it is necessary to comminute it.

Figure 7 presents the particle size distribution of the Al–TiB<sub>2</sub> metal matrix composite, SEM images of its particles, as well as an EDX analysis of the surface structure of these particles. The particle size after milling ranges from 0.5 to 95 μm, and their average size is 42.3 μm. The powder particles are fragmented, and their surface consists of TiB<sub>2</sub> inclusions.

The obtained powder can be used as the main raw material or additive in SLS, vacuum sintering, and hot pressing. In addition, the plasma-spheroidizing method can be used for this powder to improve its flow through a nozzle during fabrication [31].

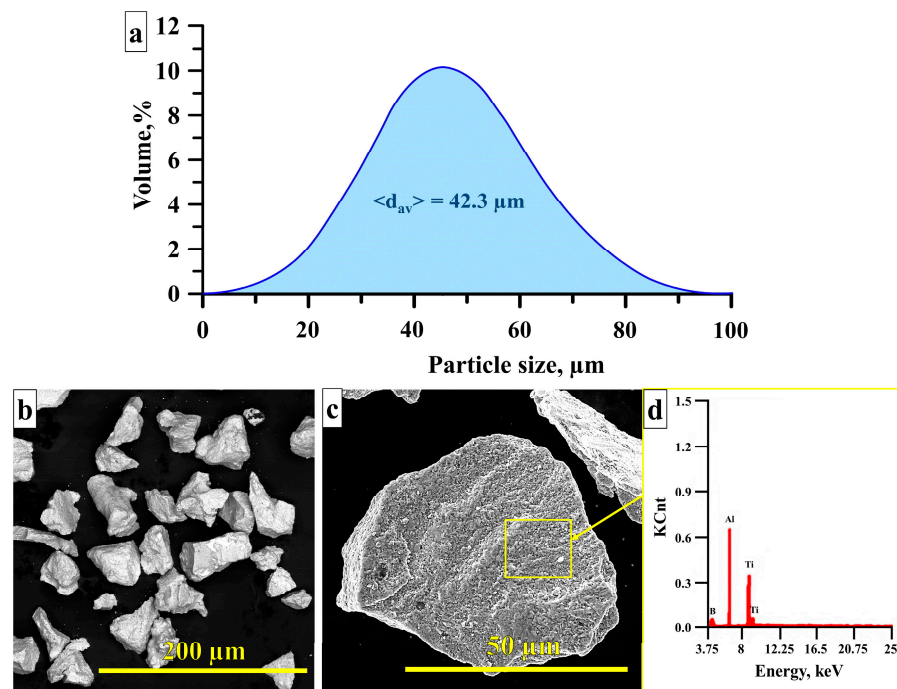


**Figure 7.** Particle size distribution (a) and SEM images (b,c) of particles in Al-TiB<sub>2</sub> metal matrix composite, EDX of the surface structure of the particles of the crushed composite (d).

#### 4. Conclusions

This work investigated the structure and phase composition of the Al-TiB<sub>2</sub> metal matrix composite produced from the Al-Ti-B system powder in semi-industrial SHS conditions. In total, 1000 g of the Al-Ti-B system powder (60 wt.% Al) was mechanically blended in a ball mill. The obtained mixture was placed in the graphite crucible without a preliminary compaction. The synthesis process was performed in the constant pressure reactor in argon medium. Summing up the results, it can be concluded that:

- The synthesis temperature in 1000 g of the Al-Ti-B system powder was 200 °C higher than that in 20 g samples synthesized in laboratory conditions;
- The final product did not differ from that obtained in laboratory conditions, and consisted of the Al matrix and TiB<sub>2</sub> ceramic particles. There were, however, Al<sub>3</sub>Ti intermetallic particles, probably due to the semi-industrial conditions of the SHS process;
- The growth in the SHS temperature provided the increase in the larger average size of TiB<sub>2</sub> particles from 0.4 to 0.6 μm, as compared to that of the laboratory samples;
- SHS-produced composite was comminuted to 42.3 μm particles, which were fragmented and had the structure inherited from the Al-TiB<sub>2</sub> composite;
- The obtained powder can be used as the main raw material or additive in SLS, vacuum sintering, and hot pressing.

**Author Contributions:** Conceptualization, A.M. and V.P.; methodology, A.M., V.P. and N.S.; validation, A.M. and V.P.; formal analysis, A.M. and V.P.; investigation, A.M., V.P., N.S., V.B. and T.T.; resources, V.P.; data curation, A.M.; writing—original draft preparation, A.M.; writing—review and editing, A.M., V.P., V.B. and T.T.; visualization, A.M.; supervision, V.P. All authors have read and agreed to the published version of the manuscript.

**Funding:** This research was funded by the Russian Science Foundation, grant number 20-79-10086-P.

**Data Availability Statement:** The data presented in this study are available on request from the corresponding author. The data are not publicly available due to private.

**Acknowledgments:** Alexey Matveev was supported by the Ministry of Science and Higher Education of the Russian Federation (public contract for the Tomsk Scientific Center of the SB RAS).

**Conflicts of Interest:** The authors declare no conflicts of interest.

## References

1. Nyamekye, P.; Golroudbary, S.R.; Piili, H.; Luukka, P.; Kraslawski, A. Impact of additive manufacturing on titanium supply chain: Case of titanium alloys in automotive and aerospace industries. *Adv. Ind. Manuf. Eng.* **2023**, *6*, 100112. [CrossRef]
2. Center, G.A.; Designs Liquid Rocket Engine Injector with 3D Systems. World Wide Web Location. Available online: <https://www.3dsystems.com> (accessed on 20 March 2024).
3. Joost, W.J. Reducing vehicle weight and improving US energy efficiency using integrated computational materials engineering. *JOM* **2012**, *64*, 1032–1038. [CrossRef]
4. Sekhar, R.; Sharma, D.; Shah, P. State of the art in metal matrix composites research: A bibliometric analysis. *Appl. Syst. Innov.* **2021**, *4*, 86. [CrossRef]
5. Cho, S.; Lee, J.; Shin, S.; Lee, D.; Kim, M.; Kwon, H.; Choi, M.; Lee, Y.S.; Jo, I.; Hong, H.U.; et al. Enhancing high-temperature properties of stainless steel composite with titanium carbide reinforcement: A study on coefficient of thermal expansion, thermal conductivity, and strength. *J. Mater. Res. Technol.* **2023**, *25*, 7241–7253. [CrossRef]
6. Khalid, M.Y.; Umer, R.; Khan, K.A. Review of recent trends and developments in aluminium 7075 alloys and metal matrix composites (MMCs) for aircraft applications. *Results Eng.* **2023**, *20*, 101372. [CrossRef]
7. Aynalem, G.F. Processing methods and mechanical properties of aluminium matrix composites. *Adv. Mater. Sci. Eng.* **2020**, *2020*, 3765791. [CrossRef]
8. Shekhawat, D.; Singh, A.; Patnaik, A. Effect of ceramic reinforcement on physical and mechanical behaviour of AL6061 metal matrix composites fabricated using stir casting technique. *Int. J. Met.* **2023**, *17*, 2207–2225. [CrossRef]
9. Han, L.; Liu, Z.; Yu, L.; Ma, Z.; Huang, Y.; Liu, Y.; Wang, Z. Effect of WC nanoparticles on the thermal stability and mechanical performance of dispersion-reinforced Cu composites. *Scr. Mater.* **2023**, *222*, 115030. [CrossRef]
10. Chen, W.; Gao, G.; Meng, X.; Zhao, X.; Jiang, Y.; Wang, M.; Li, Z.; Xiao, L. Microstructure, properties and strengthening mechanism of Cu-TiB<sub>2</sub>-Al<sub>2</sub>O<sub>3</sub> composite prepared by liquid phase in-situ reaction casting. *J. Alloys Compd.* **2022**, *912*, 165170. [CrossRef]
11. Lin, F.; Jia, F.; Ren, M.; Wang, J.; Yang, M.; Chen, Z.; Jiang, Z. Microstructure, mechanical and thermal properties of ultrafine-grained Al<sub>2024</sub>-TiC-GNPs nanocomposite. *Mater. Sci. Eng. A* **2022**, *841*, 142855. [CrossRef]
12. Xing, H.; Hu, P.; He, C.; Zhang, X.; Han, J.; Yang, F.; Bai, R.; Zhang, W.; Wang, K.; Volinsky, A.A. Design of high-performance molybdenum alloys via doping metal oxide and carbide strengthening: A review. *J. Mater. Sci. Technol.* **2023**, *160*, 161–180. [CrossRef]
13. Kota, N.; Charan, M.S.; Laha, T.; Roy, S. Review on development of metal/ceramic interpenetrating phase composites and critical analysis of their properties. *Ceram. Int.* **2022**, *48*, 1451–1483. [CrossRef]
14. Chechi, P.; Maurya, S.K.; Prasad, R.; Manna, A. Microstructural and mechanical characterization of stir cast Al-SiC/Flyash/Graphite hybrid metal matrix composite. *Mater. Today Proc.* **2022**, *64*, 637–642. [CrossRef]
15. Li, X.; Zhang, M.; Zhang, G.; Wei, S.; Xu, L.; Zhou, Y. Effect of spark plasma sintering temperature on structure and performance characteristics of Cu-20wt% W composite. *J. Alloys Compd.* **2022**, *912*, 165246. [CrossRef]
16. Durlu, N. Titanium carbide based composites for high temperature applications. *J. Eur. Ceram. Soc.* **1999**, *19*, 2415–2419. [CrossRef]
17. Levashov, E.A.; Mukasyan, A.S.; Rogachev, A.S.; Shtansky, D.V. Self-propagating high-temperature synthesis of advanced materials and coatings. *Int. Mater. Rev.* **2017**, *62*, 203–239. [CrossRef]
18. Matveev, A.; Promakhov, V.; Schulz, N.; Bakhmat, V.; Belchikov, I. Structure and phase composition of SHS composites based on Al-Ti-B system with different Al content. *Ceram. Int.* **2024**, *50*, 503–511. [CrossRef]
19. Promakhov, V.; Matveev, A.; Schulz, N.; Grigoriev, M.; Olisov, A.; Vorozhtsov, A.; Zhukov, A.; Klimenko, V. High-temperature synthesis of metal-matrix composites (Ni-Ti)-TiB<sub>2</sub>. *Appl. Sci.* **2021**, *11*, 2426. [CrossRef]
20. Matveev, A.; Promakhov, V.; Schulz, N.; Bakhmat, V.; Babaev, A.; Semenov, A.; Vorozhtsov, A. Effect of the mass fraction of NiTi-TiB<sub>2</sub> SHS-particles on the phase composition, structure, and mechanical properties of Inconel 625-NiTi-TiB<sub>2</sub> composites produced by direct laser deposition. *Materials* **2022**, *15*, 6861. [CrossRef]
21. Matveev, A.; Zhukov, I.; Ziatdinov, M.; Zhukov, A. Planetary milling and self-propagating high-temperature synthesis of Al-TiB<sub>2</sub> composites. *Materials* **2020**, *13*, 1050. [CrossRef]
22. Maslov, V.M.; Borovinskaya, I.P.; Merzhanov, A.G. Problem of the mechanism of gasless combustion. *Combust. Explos. Shock Waves* **1976**, *12*, 631–636. [CrossRef]
23. Ladd MF, C.; Palmer, R.A.; Palmer, R.A. *Structure Determination by X-ray Crystallography*; Plenum Press: New York, NY, USA, 1977; p. 233.
24. Rietveld, H.M. Line profiles of neutron powder-diffraction peaks for structure refinement. *Acta Crystallogr.* **1967**, *22*, 151–152. [CrossRef]
25. Borovinskaya, I.P.; Merzhanov, A.G.; Novikov, N.P.; Filonenko, A.K. Gasless combustion of mixtures of powdered transition metals with boron. *Combust. Explos. Shock Waves* **1974**, *10*, 2–10. [CrossRef]
26. Yeh, C.L.; Chen, W.H. Preparation of niobium borides NbB and NbB<sub>2</sub> by self-propagating combustion synthesis. *J. Alloys Compd.* **2006**, *420*, 111–116. [CrossRef]
27. Matveev, A.; Promakhov, V.; Schultz, N.; Vorozhtsov, A. Synthesis of metal matrix composites based on crxniy-tin for additive technology. *Materials* **2021**, *14*, 5914. [CrossRef]

28. Lubarda, V.A. On the effective lattice parameter of binary alloys. *Mech. Mater.* **2003**, *35*, 53–68. [[CrossRef](#)]
29. Gu, Y.; Qian, Y.; Chen, L.; Zhou, F. A mild solvothermal route to nanocrystalline titanium diboride. *J. Alloys Compd.* **2003**, *352*, 325–327. [[CrossRef](#)]
30. Lewis, D.; Wheeler, E.J. The effect of temperature on microstrains and crystallite growth in alumina. *J. Mater. Sci.* **1969**, *4*, 681–684. [[CrossRef](#)]
31. Liu, B.; Duan, H.; Li, L.; Zhou, C.; He, J.; Wu, H. Microstructure and mechanical properties of ultra-hard spherical refractory high-entropy alloy powders fabricated by plasma spheroidization. *Powder Technol.* **2021**, *382*, 550–555. [[CrossRef](#)]

**Disclaimer/Publisher’s Note:** The statements, opinions and data contained in all publications are solely those of the individual author(s) and contributor(s) and not of MDPI and/or the editor(s). MDPI and/or the editor(s) disclaim responsibility for any injury to people or property resulting from any ideas, methods, instructions or products referred to in the content.